International Journal of Advanced Engineering and Technology
ISSN: 2456-7655; Impact Factor: RJIF 5.54
Received: 17-01-2019; Accepted: 20-02-2019
www.newengineeringjournal.com
Volume 3; Issue 2; March 2019; Page No. 27-37

Mechanical properties of bending 3DP models of different thickness infiltrated with alternative materials

Edwin Ocaña-Garzón[1*], Jorge Lino Alves[2]
[1] Departamento de Ciencias de la Energía y Mecánica, Universidad de las Fuerzas Armadas–ESPE, Sangolquí, Ecuador
[1, 2] INEGI, Faculty of Engineering, University of Porto, Porto, Portugal

Abstract
Binder jetting is a well-established three-dimensional printing (3DP) process to produce models with different purposes. These prototypes need to be infiltrated to increase the mechanical resistance, but depending on the type of infiltrant and models thickness, the penetration depth varies, and consequently their strength. In this research, three types of epoxy resins with dissimilar viscosities were selected to determine their influence on the flexural properties of the models, and evaluate the correlation between thickness and type of infiltrant. The molecular structure, viscosity and flexural strength of the resins were firstly characterized, and then 3DP bending samples with 2.5, 3.2 and 9.0 mm thickness were infiltrated by full immersion, and cured to the same conditions as the pre-tested resin samples. The infiltrated 3DP samples were characterized in terms of their porosity reduction and flexural properties. The results obtained allow to conclude that the thickness of the samples has the most significant effect on the flexural strength, while for flexural modulus, the contribution of resin type is more important. For better results, the amount of resin retained in the parts should be maximized, noting that, for thicknesses greater than 3.2 mm low viscosity resins perform better, while for thinner thicknesses, resins of moderate viscosity seem to be more adequate. It was concluded that infiltrates with short pot life could be better to avoid post-drainage of the infiltrant.

Keywords: 3D printing, infiltration, flexural properties, epoxy resin, binder jetting

1. Introduction

Additive Manufacturing (AM) revolutionized the way of thinking about manufacturing processes. AM processes in the last decade were characterized by an exponential growth that is coupled not only with different manufacturing mechanisms´ capacities of adding successive layers in different materials but also with the expiration of the first patents. Nowadays, there is no doubt that this family of manufacturing processes is capable of producing freeform parts with topological optimization in almost any type of material [1-3].

Binder Jetting (BJ) process, commonly known as three dimensional printing (3DP) [2], has the advantage of printing models (sometimes in full colour) for different industrial sectors, which are extremely important in new products development and easily materialization of ideas. Regarding the strength of these 3DP models, especially in plaster-based materials, the resulting products may be porous [4], brittle and easily damaged [5]. So, a post-processing (PP) is usually demanded to produce parts with enough mechanical strength, shiny appearance and other technological characteristics [6].

Two of the most commonly used PP for BJ are sintering and infiltration [7], with the latter being the most popular due to its simplicity [8]. Infiltration is a way to achieve higher density [9], and improve, among others, the mechanical properties of the 3DP green parts, where its quality basically depends on the type of infiltrant [10] and its process. There are different infiltration techniques, either by simple immersion, with or without vacuum, drip, brush, or spray [7, 11]. These processes selection depends on the type of infiltrant and the specific objective of the 3DP model.

An ideal infiltrant should completely fill the porous space, and exhibit good flow and wetting of the pore structure. For 3DP parts in plaster-based materials, the infiltrant must be in a liquid state (but not aqueous) as it would react with the plaster [8].

Two infiltrants commonly used are cyanoacrylates and resins [12]. Cyanoacrylates have an excellent ability to penetrate the pores, thanks to their low viscosity, but their rapid polymerization makes them brittle materials [13], and beyond that they have toxicity problems [5]. Epoxy resins have an excellent combination of mechanical and chemical properties, turning them one of the most important thermosetting polymers, used in a wide range of applications [14], some dedicated to infiltrate 3DP models.

The infiltrant must penetrate into the model but, depending on its type and model thickness, different penetrations can be achieved [13], and consequently the mechanical strength that the model can withstand also changes [15]. However, this (binomial) combination, infiltrant and model thickness, should be furtherly studied, to optimize the infiltration process.

The majority of the research concerning BJ have explored the printing properties of this technology [7, 16-22], but only few studies (Table 1) are devoted to PP and, and within these, the penetration of the infiltrant into the model, leaving the relation with the final bending properties not discussed in depth.

Table 1 presents the main achievements of some research studies concerning the effects of the infiltration process on the mechanical properties of 3DP parts in plaster-based materials. The first publications that relate the effects on the mechanical properties of infiltrated 3DP parts with epoxy resins and waxes appeared in 2004 [4, 23] in an informative way.

Table 1: Previous studies of 3DP parts in plaster materials, after infiltration, produced by BJ

		Printing Parameters			Infiltration				Mechanical Effects			Infiltration
		Layer thickness	Built Orient.	Built Position	Type	Time	Method	Absorption	Tensile	Flexural	Compression	
Ipens *et al*. [24, 25]	2016		x		x	x		x	x		x	Zmax (epoxy resin)
Galeta *et al*. [13]	2013	x	x		x				x			Loctite Hysol 9483 (epoxy resin)
Gharaie *et al*. [26]	2013	x	x		x				x			Z90 (superglue)
Pilipović *et al*. [27]	2009				x				x	x		Loctite Hysol 9483 A&B (epoxy resin)
Frascati [10]	2007		x	x	x			x	x	x		Zmax, and high temp.epoxy resin.
Suwanprateeb[28]	2007					x	x	x		x		Heat-cure acrylic, cyanoacrylate, wax
Steele *et al*. [23]	2004								x		x	Z-Max
Hackney *et al*. [4]	2004				x					x		Different viscosity waxes

3D printed parts with plaster and cellulose base-materials infiltrated with acrylic, cyanoacrylate, and wax were compared when in direct contact with water or exposed to moisture [28]. The author concluded that in humidity environments, plaster samples are not as resistant as cellulose ones, especially in direct contact with water, suggesting a careful selection of the materials system to produce models with good performance.

Frascati [10] used several infiltrants in his research and concluded that the best strength was reached with epoxy resins, and more specifically with the least viscous ones.

Pilipovic *et al*. [27] compared the final tensile and flexural strengths of 3DP parts obtained by polyjet vs. those obtained by BJ infiltrated with genuine (supplied by 3DP equipment manufacturer) and non-genuine infiltrants. The parts were analysed in terms of their printing parameters rather than their infiltration process, emphasizing that non-genuine infiltrants provide similar strengths to genuine ones.

The effects of printing build orientation, and post-processing methods on the tensile strength of 3DP parts were investigated by Gharaie *et al*. [26], finding that the highest strength was achieved by a combination of 45º direction Z90, super glue infiltration, and baking in an oven at 75ºC for 2 hours. In addition, they verified that the drying process of 3DP green parts had minimal effect on the final strength. For the same purpose, Galeta *et al*. [13], reported that the strength of 3D printed samples is mainly related with the infiltrants, but it may be further increased by selecting the best combination of layer thickness and build orientation.

Ipens *et al*. [24, 25] observed that after five minutes of complete immersion, the infiltrant no longer penetrates the printed models, regardless its viscosity, concluding that the specimens infiltrated with epoxy resins are stronger overall, and the specimens whose immersion time reached 120 seconds, were the strongest. They also concluded that 3D printer powder material does not react similarly with different materials used as infiltrants, and cannot be easily predicted from just one study.

It should be noted that, in a general way, the strength of a non-infiltrated part will be somewhat affected by build orientation; parts oriented along the X-axis and Y-axis are stronger than the ones oriented along Z-axis. Once a part is infiltrated, it uniformly takes the strength characteristics of the infiltrant product [29].

These researches seem to indicate that a clear relation between samples thickness and type of infiltrant, to reach the best mechanical properties, is still undefined. This paper tries to fill this gap studying the flexural properties of 3DP samples infiltrated with 3 different epoxy resins; two of them of general application in RTM (resin transfer moulding) and a third one recommended by 3DP manufacturers. The flexural study was selected because bending test shows the ability of the part to withstand breakdown in use; additionally, this is also a reasonable guide to tensile strength [30, 31].

This study is structured as follows: firstly, the infiltrants (pure resins) were characterized, later the plaster-based samples were infiltrated by full immersion, and the flexural properties determined. Finally, the results obtained were validated using statistical tools, and discussed

2. Materials and Methods

To evaluate the relationship between the types of resins and the different thicknesses of the 3DP samples (input -factors) and the effect on the maximum flexural strength "σ_{fM}" and flexural modulus "E_B" (output -response), the study was divided in two stages, as shown in Fig. 1; i) characterization of infiltrants, and ii) characterization of 3DP infiltrated parts.

For stage i), Fig. 1, left side, three epoxy resins were selected as infiltrants, two of them used in applications other than 3DP parts infiltration, and a third one dedicated to infiltration of 3DP plaster parts. The molecular structure, viscosity and flexural properties of each resin was determined.

For stage ii), Fig. 1, right side, a Design of Experiments (DoE) was adopted, following a full factorial methodology. Flexural samples of different thickness were printed followed by infiltration. These samples were weighed before and after infiltration to evaluate their pores reduction, and then the infiltrated samples were tested in bending. Analysis of Variance (ANOVA) was used to validate the results by calculating the means of each level, for each factor.

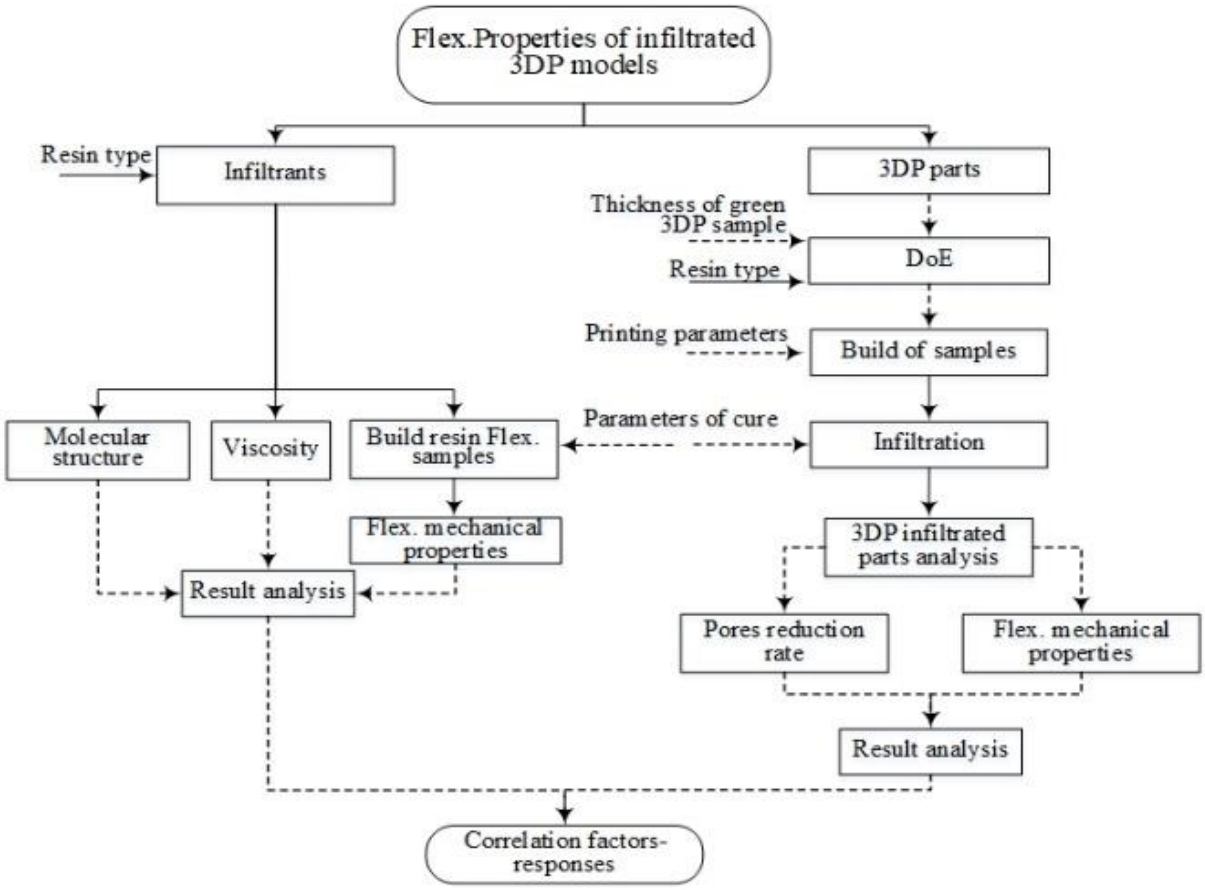

Fig 1: Diagram of research stages

2.1 Characterization of infiltrants

Three types of bi-component epoxy resins were selected. One of them, commercially known as Strength Max (3D Systems Inc., USA), is basically constituted by 3-aminomethyl-3,5,5trimethylcyclohexylamine and benzyl alcohol [32], henceforth referred as *E1* (used as reference for this study). The two other resins are basically composed by a bisphenol-A-(apichlorhydrin) and epoxy [33, 34]; a Biresin CR83 and a catalyst CR83-6 (Sika, Germany), hereinafter called *E2*, and a EC131LV and hardener W342 (Elantas, Germany), designated *E3*.

These resins were selected considering the basic characteristics that an infiltrant must meet [8]. Their typical physical data are shown in Table 2, and their viscosities are highlighted: low for *E1* and *E2*, and medium for *E3*. Resins *E2* and *E3* are commonly used in RTM, therefore, are readily available. The *E1* resin was designed exclusively for the infiltration of the 3DP plaster-based models.

Table 2: Main physical data of the infiltrants [32-34]

Characteristic	Strength Max	Biresin CR83-6	EC131LV / W342
Code assigned	**E1**	**E2**	**E3**
Applications and characteristics	Infiltration of 3DP parts of plaster base powder to improve high strength	Infusion and injection of complex and thin geometries	Good surface finish, very good resistance to UV
Colour	clear	colourless to yellowish	violet to colourless
Mix ratio parts by weight	5:2	10:3	10:2.5
Viscosity, 25ºC (resin) (m.Pa)	-	510	1000-1600
Viscosity, 25ºC (mixed) (m.Pa)	120	170	-
Density, 25ºC (mixed) (g.cm^{-3})	0.94	1.15	1.08 – 1.12
Pot Life (min)	45 for 500 g*@23ºC	180 for 100g@RT	22-32; 100 ml @25ºC
Cure time	2h@70ºC / 24h@23ºC	8h@70ºC / 12h@55ºC	24h@RT+15h@60ºC

The Fourier-transform infrared (FTIR) spectroscopy analysis was performed in a 630 FTIR spectrometer (Agilent Cary, USA), to identify and compare at the molecular level, both the resins, and the mixture of these with their respective curing agent (hereafter called "mix-resin"). This test was carried out using the path–length attenuated total reflectance (path–length ATR) technique, and the spectra was obtained at a frequency range of 4000 to 650 cm^{-1}, with 4 clean scans and 140 background scans, resolution 4 cm^{-1}.

The viscosity (ν) and the pot life of the mix-resins were also measured. The two components were manually pre-mixed for two minutes just before the test. A tuning fork vibrator

viscometer model SV-10 (A&D, Japan) was used at natural frequency of 30 Hz within the sample fluid. The amount of resin was enough to keep the two thin plates sensors submerged in them. Each resin was tested for at least 30 minutes.

In order to independently know the flexural performance of the resins, and then understand their behaviour as infiltrants, five specimens (127.5 x 12 x 3.2 mm) of each resin were cast in open silicone moulds, as suggested in reference [35] for resins without fillers and methods of static cure. All samples were cured at room temperature (RT, 23±1 ºC) for 24 h., and post-cured in a forced air convection oven SLW53 STD (PolEko, Poland) at 70 °C for 2.5 h. These cure conditions were selected based on the suggestions of the resin manufacturers, but adjusted to a single condition, focusing on obtaining the shortest process time without affecting their final mechanical properties. Finally, three-point bending tests were carried out at RT, according to ASTM D790, in a universal testing machine with a 10 kN load cell (MTS 810, USA). The samples were supported by two rods of 5 mm radius with a span of 50 mm, and loaded by an upper rod of 4 mm radius. The crosshead load speed was set at 2 mm/min.

2.2 Characterization of infiltrated 3DP samples

A DoE was employed to identify the influence of the factors, resin type and thickness of the sample, on the maximum flexural strength (σ_{fM}), and E-flexural modulus (E_B) of the 3DP infiltrated samples with the previously characterized resins. For each of these two factors, three levels were analysed, as shown in Table 3. The geometry recommended by ASTM D790 was adopted to define the sample thickness of 3.2 mm (*C2*). Two more thicknesses were also selected: one slightly thinner, of 2.5 mm (*C1*), and a thicker one with 9.0 mm (*C3*) (see Table 3). Based on a full factorial design and the number of factors and levels, an arrangement of 9 factors combinations was obtained, where *YE1*, *YE2* and *YE3* correspond to 3DP specimens infiltrated with resins *E1*, *E2* and *E3*, respectively (Table 4). The tests were performed with five samples for each combination, resulting in a total of 45 specimens.

Table 3: Factors and assigned levels for DoE of 3DP samples

Factors	Levels		
	1	2	3
Resin type	YE1	YE2	YE3
Thickness of the 3DP sample (mm)	C1=2.5	C2=3.2	C3=9.0

Table 4: Tested factors with full factorial DoE and their corresponding assigned codes

Combination	Factors		Assigned code
	Resin type	Thickness of the 3DP sample (mm)	
1	E1	C1=2.5	YE1-C1
2	E2	C1=2.5	YE2-C1
3	E3	C1=2.5	YE3-C1
4	E1	C2=3.2	YE1-C2
5	E2	C2=3.2	YE2-C2
6	E3	C2=3.2	YE3-C2
7	E1	C3=9.0	YE1-C3
8	E2	C3=9.0	YE2-C3
9	E3	C3=9.0	YE3-C3

To avoid the influence (noises) of other parameters that are not under study, both the printing and infiltration parameters were adjusted and kept constant. The printing parameters were selected according to the 3DPrint software default values that are suitable for most part geometries [29]: binder saturation level at 100%, binder/volume ratios, 0.24 for shell and 0.12 for core, printing layer thickness of 0.01 mm, and vertical building speed of 28mm/h. The printing materials are plaster-based powder, commercially known as VisiJet® PXL Core [36], and water based binder solution VisiJet® PXL [16, 37]. The 3DP samples were manufactured by batches according to their thickness on a 3D printer Projet 660 Pro (3D Systems, USA), in a build position and orientation shown in Fig. 2. The build position and orientation were selected for a maximum build speed by placing the samples with the smallest dimension along the Z-axis (this is automatically detected by the 3DPrint software V1.0). After printing, the samples were dried at 70ºC for 2 h. in the same build chamber.

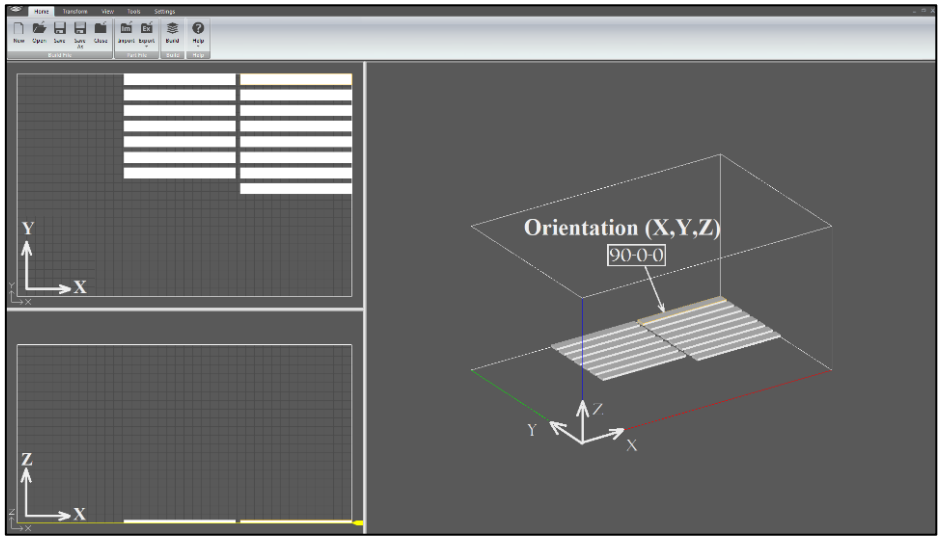

Fig 2: Build position and orientation of a batch of samples in the 3D printer chamber

To determine the infiltrant absorbed by the 3DP samples, porous reduction rate (*RP*) was determined according to Eq. (1). For this, samples were weighed in a HDL-300 (Scale House, USA) precision scale, before ("m_b" - bulk mass before infiltration) and after infiltration and cure ("m_a"), respectively. The real mass "m_r", was estimated assuming a

totally compact theoretical mass according to Eq. (2), where, δr is the real density of the printing powder (2.6 g/cm3) [36], and V_r is the CAD dimensions of the samples, where width "*w*", thickness "*t*" and length "*L*" are shown in Table 5. Considering that the resins have similar densities (see Table 2), it was assumed that $m_{aE1} = m_{aE2} = m_{aE3} = m_a$.

$$RP = \frac{m_r - m_b}{m_r - m_a} \text{ Eq.} \quad (1)$$

$$m_r = V_r . \text{ Eq.} \quad (2)$$

Table 5: Real mass and volume obtained from theoretical samples dimensions

Density, ρ_r (g/cm^3)	CAD dimensions, *wxtxL* (mm)	Volume, *Vr* (cm^3)	Mass, *mr* (g)
2.6	C1: 10.0x2.5x60.0	1.50	3.90
	C2: 12.7x3.2x127.0	5.16	13.42
	C3: 12.7x9.0x165.0	18.86	49.03

The infiltration of the 3DP samples was performed by the full immersion method, following the conditions indicated in Table 6. The immersion time was selected to five minutes, because this type of infiltrants are not able to further penetrate into the samples at atmospheric conditions [24, 25]. It is worth noting that both cure and post-cure conditions were the same as the ones used for full resin bending samples.

Table 6: Parameters for infiltration of samples by full immersion

Parameter (units)	Values
Mixing time of resin parts (min)	2
Immersion time (min)	5
Cure, time - temperature (h @ ºC)	24 @ RT*
Post cure, time – temperature (h @ ºC)	2.5 @ 70

**RT: 23 ±1ºC*

For each resin, the two components were manually mixed according to the ratios indicated in Table 2. Batches of 300 ml were selected to have enough volume to fully immerse the specimens. The mixture was poured into a container and the specimens (Table 5) were immersed for 5 min., and then removed and allowed to cure on wax paper for 24 h. at RT and baked for 2.5 h. at 70°C. After cooling, the samples were stored in an airtight container until the mechanical tests.
A three-point bending test was performed according to ASTM D790-10 in the same equipment previously described. The support span was set at 40, 50, and 135 mm for samples thicknesses of 2.5, 3.2 and 9.0 mm, respectively.

3. Results & Discussion

3.1 Characterization of resins

The spectra of the resins (bases) Fig. 3 a), and the mix-resins, Fig. 3 b), are presented cut between the amplitudes of 2750 and 1700 cm^{-1} because in range no peaks were detected.
The resemblance of the pure resin spectra (Fig. 3 a)) indicate a similar molecular structure of the three primary components of each resin. The main difference is shown at 753 cm^{-1}, where the resin *E1* stood out as the highest.
The spectra of the mix-resins show noticeable differences, especially for *E3* (Fig. 3 b)), where all peaks are lower than *E2* and *E1*, with more pronounced differences in the bands of 1508, 1182, 828 and 753 cm^{-1}, suggesting that the type of catalyst for *E3* has more differences in the molecular bonds concentration, as claimed by Tripathi and Srivastava [38].
The reflectance band in Fig. 3 b) at 3500 cm^{-1}, refers the presence of ν OH on uncured epoxy-amine system of diglycidyl ether of bisphenol-A (DGEBA) [39, 40], while the peak at 2925 cm^{-1} is attributed to the –CH_2– stretching. The reflectance peaks for the aromatic C–H were also detected at 1585, 1508, 753 and 667 cm^{-1}. The more intense peak at 667 cm^{-1} for resin *E2*, can be related with its great pot life [41]. The peaks shown at 1297 cm^{-1} are related with the P=N bound [41]. The inflection at 1182 cm^{-1} is linked to the C–O stretching of aromatic ring [14] of the epoxy resin, and at 913 and 828cm^{-1} indicate the presence of epoxy groups on uncured epoxy system of DGEBA [14, 38-40, 42].
The results of resins viscosity, flexural strength, and flexural modulus are summarized in Table 7 showing their averages, standard deviations, and coefficients of variation, as well as the ratios of resins *E2* and *E3* to *E1*.

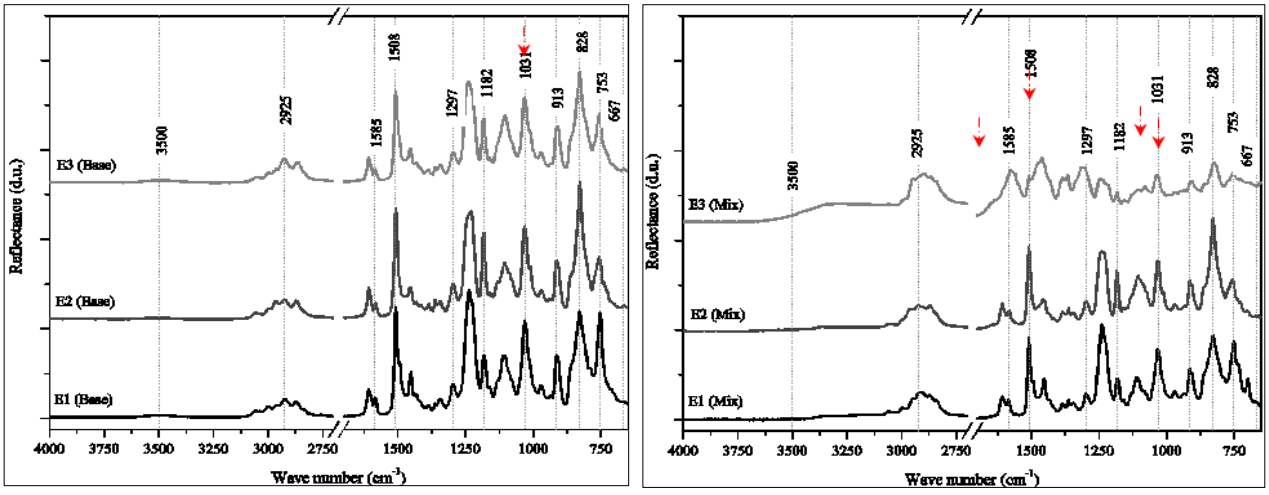

Fig 3: FTIR spectra of uncured epoxy resins *E1*, *E2*, and *E3*, for; a) base, and b) mix-resins

The viscosity at RT as a function of time of the uncured mix-resins are presented in Fig. 4, where a strip of the first fifteen minutes is highlighted (time required to infiltrate all batches of specimens). The average viscosities for this period are: 289.38, 238.04, and 980.74 mPa.s for *E1*, *E2* y *E3*, respectively. This result shows that resin *E2* is almost 18% less viscous and *E3* is 240% more viscous than the reference resin *E1* (see Table 7). The small resins viscosity standard

deviation and CV means that they have a stable viscosity for the required time (15 minutes) of the infiltration process.

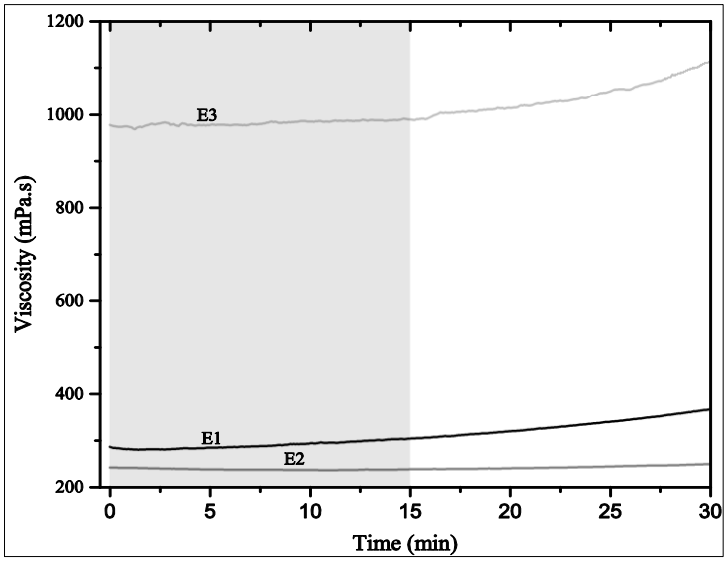

Fig 4: Viscosity "ν" at RT as a function of time of uncured mixed-resins *E1, E2* and *E3*

Table 7: Viscosity, flexural strength and flexural modulus of epoxy resins, average with standard deviation and coefficient of variation (%)

Type of resins	Resin Viscosity, "ν" (mPa.s) at RT.			Max. Flex. Strength, "σ_{fM}" (MPa)			E-Flex. Modulus, "E_B" (GPa)		
E1	289.38	±7.26	3%	112.38	±2.34	2%	3.01	±0.09	3%
E2	238.04	±1.54	1%	105.40	±5.26	5%	3.11	±0.07	2%
E3	980.74	±5.00	1%	61.68	±18.01	29%	3.42	±0.12	4%
E2 / E1	0.82			0.94			1.03		
E3 / E1	3.39			0.55			1.14		

The highest flexural strength was obtained with *E1* resin (112.38 MPa), which is 6% higher than *E2* and 45% than *E3*, while for flexural modulus, *E3* resin exhibits the largest modulus. This ratios are collected in Table 7 depicted in Fig. 8Error! Reference source not found.

Comparing these results with the manufacturer data sheets (with other cure conditions) [33, 34], resins *E2* and *E3* reached 84% and 56% of their claimed flexural strength, while for modulus was 93% and 122%. These results highlight that resin *E3* was the most affected with the selected processing conditions.

The decrease in the resistance of *E3* resin might be due to small air bubbles trapped inside the flexural samples, which were more difficult to eliminate due to its higher viscosity, while the increase in the modulus, among other factors, could be a consequence of the fast cooling rate occurred after post-cure. According to the glassy state theory, there is an exponential relaxation of the process of a specific volume with time [43, 44], therefore, the increase in modulus is directly related to the decrease in free volume available for segmental mobility [45].

3.2Characterization of the infiltrated 3DP samples

The *RP*, flexural strength and flexural modulus results of the infiltrated 3DP samples are summarized in Table 8, which shows the averages and standard deviations for full 9 combinations of resin type vs. thickness of the samples.

According to the Eq. (1), if $m_a \rightarrow m_b$ (masses of the 3DP samples before and after the infiltration) there is no significant infiltration, i.e. no pore reduction occurs ($RP = 1$). *RP* is higher than one when m_a. is greater than m_b. In this context, Table 8 and Fig. 5 show a *RP* reduction for each combination type of resin—thickness of the sample. In general, a higher pore reduction rate (more infiltration) occurred in 2.5 mm infiltrated models (*C1*), being the higher value (1.56) reached in *YE3-C1*.

Table 8: Experimental results of mass measurements, *RP*, σ_{fM}, and E_B of 3DP infiltrated samples (average and standard deviation for each condition)

Combination	Code	m_b (g)		m_a (g)		*RP*		σ_{fM} (MPa)		E_B (GPa)	
1	*YE1-C1*	1.85	±0.01	2.43	±0.04	1.40	±0.04	35.39	±0.68	6.63	±0.18
2	*YE2-C1*	1.85	±0.02	2.49	±0.02	1.45	±0.02	41.46	±1.00	7.15	±0.32
3	*YE3-C1*	1.88	±0.04	2.60	±0.08	1.56	±0.07	35.02	±1.74	5.58	±0.71
4	*YE1-C2*	6.51	±0.06	8.49	±0.03	1.40	±0.02	32.63	±4.67	5.62	±0.68
5	*YE2-C2*	6.59	±0.06	8.47	±0.05	1.38	±0.01	35.14	±1.96	6.82	±0.43
6	*YE3-C2*	6.63	±0.05	8.38	±0.10	1.35	±0.03	30.60	±1.61	5.91	±0.17
7	*YE1-C3*	23.11	±0.32	29.79	±1.22	1.35	±0.08	24.48	±2.51	7.24	±0.45
8	*YE2-C3*	22.78	±0.18	29.93	±0.17	1.37	±0.02	25.25	±0.85	7.85	±0.48
9	*YE3-C3*	22.90	±0.20	28.79	±1.21	1.29	±0.07	22.96	±1.95	6.03	±0.84

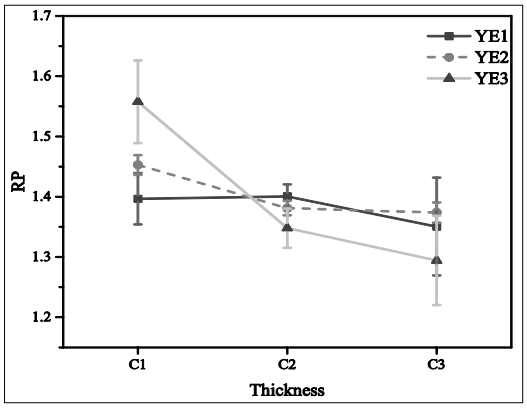

Fig 5: Pores reduction rate (*RP)* versus thickness of 3DP infiltrated samples

For the flexural strength, Fig. 6a), the highest and lowest strength was reached for 2.5 and 9.0 mm samples. Considering the same thickness, the maximum and minimum strength was achieved in samples infiltrated with resins *E2* and *E3*. This trend was kept for all thicknesses. For the modulus Fig. 6b), the tendency is different for all thicknesses, with a more dependency on the resin type instead of the thickness of the samples, where the parts infiltrated with resin *E2* have higher modulus, whereas the resin *E3* maintains the lowest modulus.

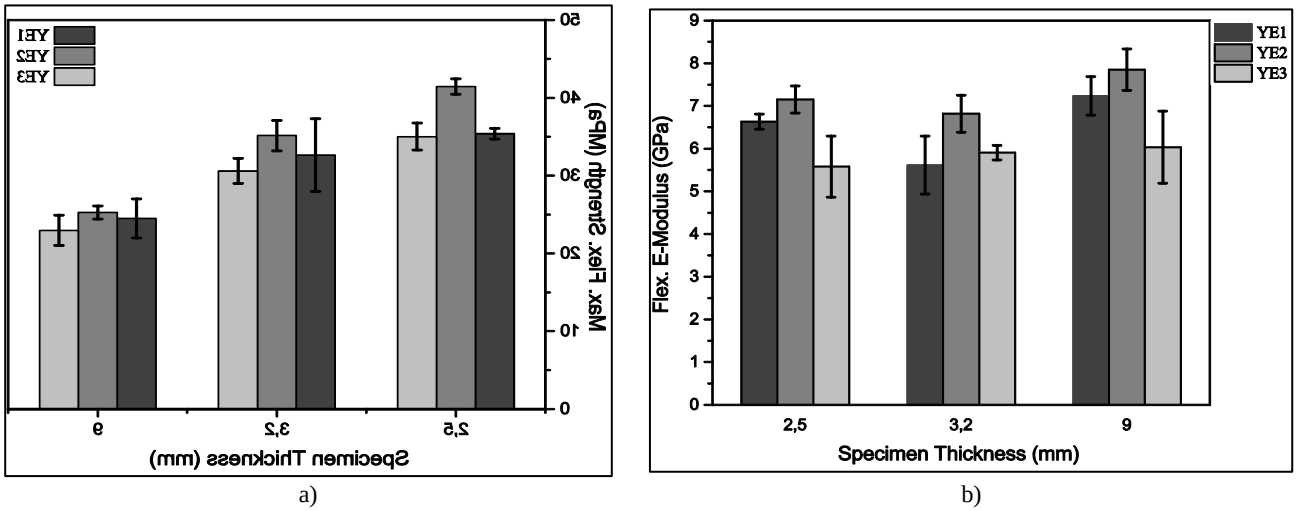

a) b)

Fig 6: Experimental results of; a) σ_{fM}, and b) E_B for 3DP infiltrated samples, (averages and standard deviations)

The factors, type of resin and thickness of the sample, as well as the obtained properties in Table 8 of σfM, E_B, and *RP*, were all analysed through ANOVA, with a 95% confidence interval (95% ci), i.e. significance level of $\alpha = 0.05$ (when $P \leq \alpha$, there are a significance effect on the response).

The ANOVA performed for *RP* between the "resin type" and "thickness sample" factors, showed the following:

The thickness sample factor has the major contribution (43.46 %), followed by its interaction with the resin type (28.41%), both cases with P = 0.000. This result means that the thickness is a highly sensitive factor, while the resin type represents no significant contribution. It is worth nothing that the contribution of the resin is not statistically significant, so its contribution should be added to the contribution of the error, the total will be 28.13%.

Analysing the main effect of the *RP* (see Fig. 7 a)) for resin type, it can be seen that there are no significant statistical differences among them. However, when the thickness of the samples is analysed, figure shows the highest *RP* = 1.469 for 2.5 mm, making it significantly different relatively to 3.2 and 9.0 mm (with these last ones statistically equal to each other). Focusing on the interaction of the two factors, *YE3-C1* shows a superiority with *RP* =1.56, followed by *YE2-C1* with *RP* =1.45, being *RP* lower in *C3* for all the infiltrants.

Higher resistance was reached with upper *RP*, on one hand with the smaller thickness (2.5 mm), and on the other hand with the more viscous resin (*E3*). This viscosity effect is in opposition with Frascati [10] and Ipens [24, 25] results, at least for thinner thicknesses and a 980 mPa.s viscosity. This behaviour can be justified because in small thicknesses a high viscosity resin still penetrates the sample, but is more difficult to spill after penetration, thanks to its greater surface tension, which allows retaining more resin inside the sample. Another factor that contributes to this phenomenon is the short pot life of the resin *E3*, giving less time to drain.

Concerning to ANOVA results obtained for the flexural strength (σf_M)

The thickness sample factor shows a major contribution (78.08 %), and a considerably minor influence of the resin (just 9.17%). In this case, these two factors are statistically significant (P = 0.000). The thickness is again the most influential factor.

The *YE2* condition, with mean of 33.95 MPa has the higher strength, however is statistically different to *YE1* and *YE3*, with these ones being statistically equal to each other (see

Fig. 7b)). The *YE2* condition (2.5 mm) is superior for all thicknesses, although *E2* resin itself does not have the greater resistance. This lower viscosity resin fills a large percentage of pores (see Fig. 5), which is crucial for the thicker sample "*C3*" (see Table 8). This is consistent with the results published by Suwanprateeb *et al*. [46], indicating that the flexural strength and modulus increase with a decreasing percentage of soluble matter present in the infiltrant (lower viscosity resin).

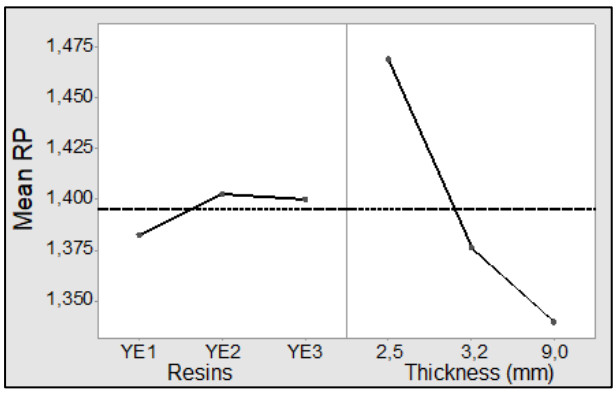

(a)

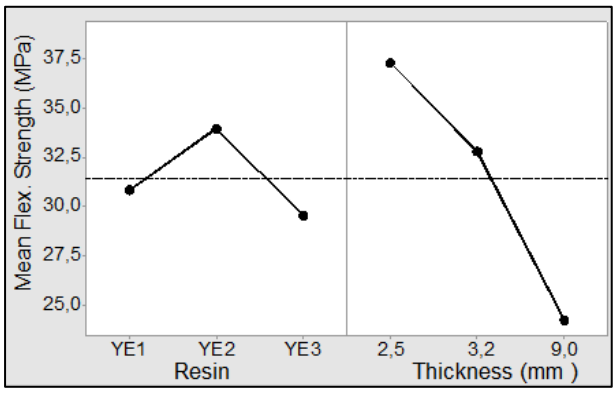

(b)

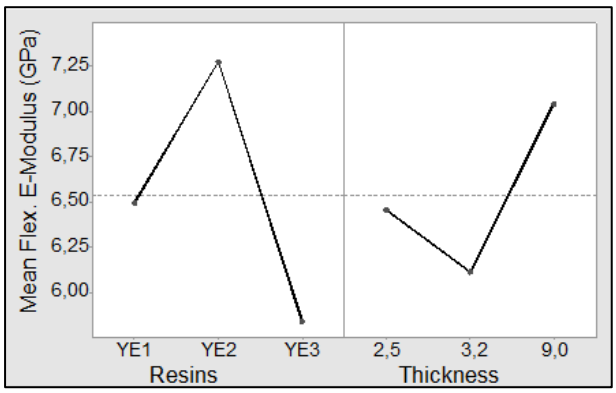

(c)

Fig 7: Means of a) reduction pore (*RP*), b) flexural strength (σf_M) and c) flexural modulus (E_B) of infiltrated 3DP samples, obtained from the ANOVA for input factors: "resin type" and "thickness sample".

Considering the analysis by thickness of the sample (Fig. 7 b)), it can be seen that the highest strength was reached with 2.5 mm test samples, followed by 3.2 and 9.0 mm, respectively, verifying that all conditions are significantly different from each other. This behaviour is similar to RP (Fig. 7 a)), so it can be considered that the flexural strength, as a function of the thickness, is proportional to the rate of pore reduction.

Finally, the ANOVA for the flexural modulus (E_B), showed: A larger contribution of the "resin type" (43.68%), followed by the thickness of the sample (18.66%). For both, P = 0.000 was obtained, and the interaction of the two factors is P = 0.026, which make them statistically significant and with more balanced contributions than the above results.

The highest modulus, considering the type of infiltrant, was obtained in the 3DP samples *YE2* (7.27 GPa), as shown in Fig. 7 c), while for thickness, was 7.04 GPa, obtained with 9.0 mm, re-confirmed again that *YE2* specimens have the highest modulus for all the thicknesses, and within these specimens, the 9.0 mm ones reached the maximum value with 7.78 GPa.

Fig. 7 c) shows a very interesting result; for thicknesses greater than 3.2mm (more porosity), the modulus increases (more brittle samples). This result is consistent with what was reported by Biswas [47] that claims the flexural modulus of plaster materials shows a linear relationship with porosity.

This experimental work allowed to conclude that the thickness of the samples has a greater influence on the flexural strength (78.08%), while the resin affects more significantly the modulus (43.68%) and, to a lesser extent, the thickness of the sample (18.66%). Therefore, the following part will analyse this subject more deeply.

Fig. 8 and Table 9 compares the strength of the infiltrated 3DP samples and the resins. *E3* resin, although less resistant (55% of *E1* – reference resin) and more viscous (240% of *E1*), is the one that generates a greater gain (ratio) in terms of transfer of its flexural strength to the post-infiltrated printed parts (from 0.37 to 0.57, according to last column in bold). The flexural strength of green 3DP plaster parts (no infiltrated) is so low around to 3 MPa, as shown in a previous study [48], so, their effect can be considered negligible for this analysis [49].

Table 9: Ratios (3DP models over resins) of flexural strength and flexural *E*-modulus

3DP thickness (mm)	flexural strength ratios			flex. E-modulus ratios		
	YE1 / E1	YE2 / E2	YE3 / E3	YE1 / E1	YE2 / E2	YE3 / E3
2.5	0.32	0.39	**0.57**	2.21	**2.30**	1.63
3.2	0.29	0.33	**0.50**	1.87	**2.20**	1.73
9.0	0.21	0.24	**0.37**	2.41	**2.53**	1.76

Considering the above results, it seems that to reach high flexural strengths in infiltrated 3DP models, it is advisable high strength infiltrants, however their effect can be attenuated due to the thickness and infiltration conditions.

For thicknesses greater than 3.2 mm, low viscosity resins to penetrate the inner pores are advisable, however for smaller thicknesses it is convenient that the infiltrants have higher viscosity.

Fig. 8 b) and Table 9 compare the flexural modulus of the resins and the infiltrated samples, with resin *E1* having the smallest value, slightly surpassed by *E2* and *E3*. In relation to the infiltrated samples, the same pattern is discernible for each thickness, having *YE3* the smallest modulus and *YE2* the highest.

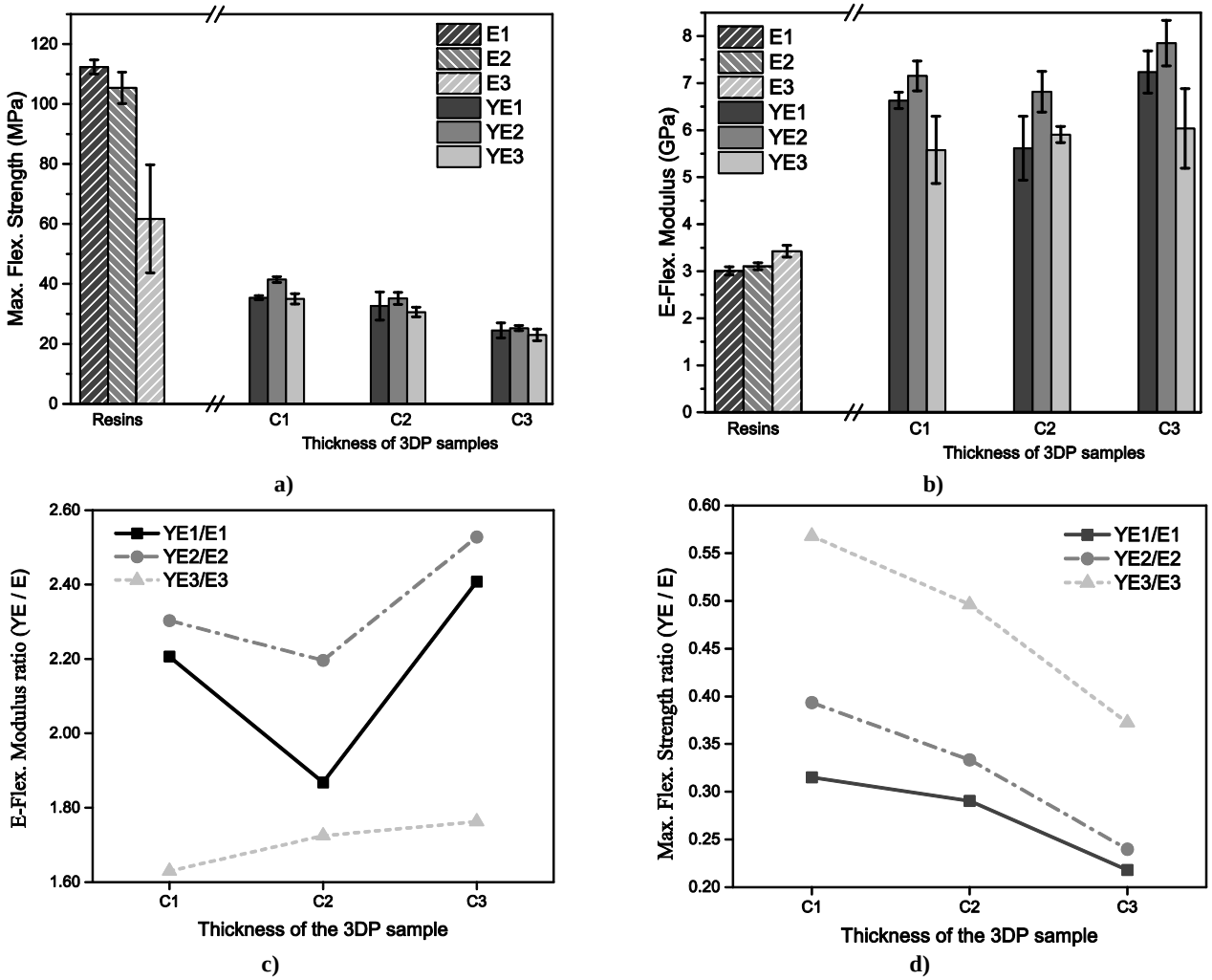

Fig 8a: Max. Flexural Strength (σf_M), and b) E-flexural modulus (E_B) of resins (*E1, E2* and *E3*) compared with infiltrated 3DP samples (*YE1, YE2* and *YE3*) by thickness (C1=2.5, C2=3.2 and C3=9.0 mm). Ratios of *YE/E* for c) σf_M and d) E_B

Comparing the ratios of 3DP samples (*YE*) versus resins (*E*) of modulus (Fig. 8 d) and Table 9), it is possible to understand that resin *E2* promotes the highest ratios from 2.30 to 2.53 (although is not the resin with best modulus). On the contrary, E3 resin, with the largest module, has the lowest ratio, from 1.63 to 1.76.

4. Conclusions

Infiltration of 3DP models, obtained by binder jetting, is a requirement to manufacture prototypes able to handle. These models can have different purposes, and for some of them, the mechanical resistance that they can withstand is very important. The present study analysed the degree of influence of three types of resin (infiltrant) on the mechanical properties of 3DP models with three different thicknesses.

All 3DP models were infiltrated by simple full immersion with epoxy resins with similar molecular structure and slight differences in their catalysts. Resin E1, of low viscosity, was selected because it is the one indicated by 3DP providers. The other two resins are common resins for Resin Transfer Moulding, of lower price and two different viscosities.

Resins *E1* and *E2* have the highest bending strength (112 and 105 MPa, respectively), while *E3* resin displaying higher viscosity, has the lowest flexural strength (62 MPa).

For the 3DP infiltrated models, the thickness has the most significant effect on the flexural strength. The higher resistance was reached with 2.5 and 3.2 mm, which is directly related to the amount of infiltrant absorbed (measured by the pore reduction rate, RP).

The type of resin had a greater effect than the thickness on the flexural modulus. The higher modulus was reached with the less viscous resin (*E2*), and within these, the 9.0 mm specimens were the ones with highest values, which made them the most brittle pieces.

In general, regarding the bending properties of the 3DP models, *E2* resin showed characteristics slightly higher than the *E1* resin (referential), while *E3* (least strength resin), showed to be the most efficient resin in transferring its properties to the 3DP models, so, these results suggest that it is feasible to use not devoted resins for successfully infiltrate 3DP parts.

In order to obtain the best mechanical properties, one must aim to increase the amount of resin retained in the part. For this, and for high thicknesses (greater than 3.2mm), it is recommended to use low viscosity resins, while for thin thicknesses (less than or equal to 3.2mm), resins of moderate viscosity are the most indicated.

For any models thicknesses, infiltrants with pot life close to the infiltration time could be better to avoid post-drainage of the infiltrated resin, and to keep the resin into the model while it polymerizes.

Another option to increase infiltrant absorbed by the 3DP model, could be the improvement of the infiltration process, through its parameters, such as temperature or pressure of

infiltration, or optimizing the cure conditions, among others.

5. Acknowledgments

This research is supported by the: Universidad de las Fuerzas Armadas ESPE, Ecuador under grant –Orden de rectorado Nº 2014-299-ESPE-a-3, and SAESCTN-PII&DT/1/2011 co-financed by Programa Operacional Regional do Norte (ON.2–O Novo Norte), under grant Quadro de Referência Estratégico Nacional (QREN); The authors also acknowledge to MSc. Leonardo Santana Sra. Beatriz Graça, MSc. Mauro Ocaña and MSc. César Narváez.

6. References

1. Gibson I, Rosen D, Stucker B. Additive Manufacturing Technologies: 3D Printing, Rapid Prototyping, and Direct Digital Manufacturing, 2014, New York: Springer 498.
2. Wohlers Report. Anual worldwide Progress Report, W. Associates, Editor. Fort Collins, CO, 2015, 1315.
3. Utela AB. Development and application of new material systems for three dimensional printing (3DP), in Mechanical Engineering. University of Washington: Washington, USA, 2008, 213.
4. Hackney PM, Channappa LC. Development of systems to increase the green part strength of the three-dimensional printed Z-Corps manufactured parts by infiltration processes to improve their range of application. in Fifth National Conference on Rapid Design, Prototyping, and Manufacturing. United Kingdom.
5. Warwick T. Method and apparatus for infusing additive manufactured objects and the like, 2016, Patent US20160067925A1: USA.
6. Sachs EM, *et al*. Three dimensional printing techniques, MIT, Editor. 1994, Patent US5340656A: USA.
7. Utela B, *et al*. A review of process development steps for new material systems in three dimensional printing (3DP). Journal of Manufacturing Processes. 2008; 10(2):96-104.
8. Zhou JG, *et al*. Low temperature polymer infiltration for rapid tooling. Materials & Design. 2004; 25(2):145-154.
9. Feenstra FK. Method for making a dental element. TNO: United States, 2005.
10. Frascati J. Effects of position, orientation, and infiltrating material on three dimensional printing models, in Department of Mechanical, Materials and Aerospace Engineering. B.S. Florida State University: Orlando, Florida, 2007.
11. Zhu J, *et al*. Water-based coatings for 3D printed parts. Journal of Coatings Technology and Research. 2015; 12(5):889-897.
12. Bredt JF, Anderson TC, Russell DB. Three dimensional printing material system and method. Z Corporation: USA, 2003.
13. Galeta Tomislav KI, Karakasic Mirko. Influence of processing factors on the tensile strength of 3d-printed models. Materiali in tehnologije. 2013; 47(6):781-788.
14. Mirmohseni-Namin A, Nikafshar S, Mirmohseni F. Increasing toughness and tensile strength of an epoxy-diamine system using an inorganic ultra-accelerator. RSC Advances. 2015; 5(65):53025-53035.
15. Junk S, *et al*. Rapid tooling in metal forming processes using 3D-printed tools. in 5th International Conference on Advanced Research in Virtual and Rapid Prototyping. Leiria, Portugal: Taylor & Francis, 2011.
16. Asadi-Eydivand M, *et al*. Effect of technical parameters on porous structure and strength of 3D printed calcium sulfate prototypes. Robotics and Computer-Integrated Manufacturing. 2016; 37:57-67.
17. Asadi-Eydivand M, *et al*. Optimal design of a 3D-printed scaffold using intelligent evolutionary algorithms. Applied Soft Computing Journal. 2016; 39:36-47.
18. Sachs EM. Powder dispensing apparatus using vibration. Massachusetts Institute of Technology United States, 2000, 26.
19. Utela BR, *et al*. Development process for custom three-dimensional printing (3DP) material systems. Journal of Manufacturing Science and Engineering. 2010; 132(1):011008.
20. Miyanaji H, *et al*. Process development of porcelain ceramic material with binder jetting process for dental applications. JOM. 2016; 68(3):831-841.
21. Shirazi SFS, *et al*. A review on powder-based additive manufacturing for tissue engineering: selective laser sintering and inkjet 3D printing. Science and Technology of Advanced Materials. 2015; 16(3):033502.
22. Zañartu-Apara G, Ramos-Grez J. Characterization of the mechanical properties of samples fabricated by an experimental SGM device. Rapid Prototyping Journal. 2010; 16(5):356-364.
23. Steele KAM, Herbert N, Pretet V. A study on the effects of resin infiltration techniques on parts produced using the three-dimensional printing process. in Fifth National Conference on Rapid Design, Prototyping, and Manufacturing, 2004, Great Britain: John Wiley & Sons Inc.
24. Impens D. An experimental approach to assess the impact of post processing variables on the mechanical characteristics of 3D printed (powder binding process) parts, in Mechanical, Automotive, and Materials Engineering. University of Windsor: Ontario, Canada, 2015.
25. Impens D, Urbanic RJ. A comprehensive assessment on the impact of post-processing variables on tensile, compressive and bending characteristics for 3D printed components. Rapid Prototyping Journal. 2016; 22(3):591-608.
26. Gharaie SH, Morsi Y, Masood SH. Tensile Properties of Processed 3D Printer ZP150 Powder Material. Trans Tech Publ, 2013.
27. Pilipović A, Raos P, Šercer M. Experimental analysis of properties of materials for rapid prototyping. The International Journal of Advanced Manufacturing Technology. 2009; 40(1-2):105-115.
28. Suwanprateeb J. Comparative study of 3DP material systems for moisture resistance applications. Rapid Prototyping Journal. 2007; 13(1):48-52.
29. 3DSystems I. 3DPrint1.0 System Software - User guide, I. 3DSystems, Editor. 3DSystems Inc.: South Carolina USA, 2013, 14.
30. Brown R. Handbook of Polymer Testing, ed. R.T. Limited. Shawbury, UK, 2002.
31. Simons EN. Testing of metals. Great Albion Books, 1972.
32. 3D Systems I, Strength Max Z. Max 90 Hardener, CAS-No 2855-13-2, I. 3D Systems, Editor. South Carolina U.S.A, 2013.

33. Sika. Biresin ® CR83 Resin, MSDS S.D. GmbH, Editor. 2014: Stuttgart.
34. Elantas EI. EC 131LV/W 342 - Product Information, E.I. Elantas, Editor. Elantas Italia S.r.l.: Germany, 2014.
35. Netto SDC. Aurélio, Desenvolvimento de compósito de resina epóxi e fibras curtas de aço para fabricação rápida de moldes para injeção de termoplásticos, in Engenharia mecânica. Universidade Federal de Santa Catarina: Florianópolis, 2008, 224.
36. 3DSystems, VisiJet PXL Core - Powder CAS-No 10034-76-1 D. Inc., Editor. 3DSystems Inc.: South Carolina USA, 2013.
37. 3DSystems. VisiJet PXL-Binder Solution CAS Nº 616-45-5, I. 3DSystems, Editor. South Carolina U.S.A, 2013.
38. Tripathi Srivastava GD. Effect of carboxyl-terminated poly(butadiene-co-acrylonitrile) (CTBN) concentration on thermal and mechanical properties of binary blends of diglycidyl ether of bisphenol-A (DGEBA) epoxy resin. Materials Science and Engineering: A. 2007; 443(1-2):262-269.
39. Romão BMV, *et al*. Characterization of the curing agents used in epoxy resins with TG/FT-IR technique. Polímeros. 2006; 16:94-98.
40. Kersting D, Wiebeck H, Esper FJ. Caracterização de resinas epóxi para compósitos curadas através de irradiação de micro–ondas. Revista Iberoamericana de Polímeros. 2015; 16(3):148-156.
41. Liu J, *et al*. Synthesis, characterization and curing properties of a novel cyclolinear phosphazene-based epoxy resin for halogen-free flame retardancy and high performance. RSC Advances. 2012; 2(13):5789-5799.
42. Sun T, Chang XL, Lai JW. Experimental studies on epoxy-amine system using microwave and conventional curing approaches. Trans Tech Publ, 2012.
43. Debenedetti PG, Stillinger FH. Supercooled liquids and the glass transition. Nature. 2001; 410(6825):259.
44. Kauzmann W. The Nature of the Glassy State and the Behavior of Liquids at Low Temperatures. Chemical Reviews. 1948; 43(2):219-256.
45. Garton A, *et al*. Additives for improving the strength, stiffness, and ductility of epoxy resins. Polymer Engineering & Science. 1987; 27(21):1620-1626.
46. Suwanprateeb J. Improvement in mechanical properties of three-dimensional printing parts made from natural polymers reinforced by acrylate resin for biomedical applications: a double infiltration approach. Polymer International. 2006; 55(1):57-62.
47. Biswas DR. Influence of porosity on the mechanical properties of lead zirconate--titanate ceramics. California Univ., Berkeley (USA). Lawrence Berkeley Lab, 1976.
48. Ocaña GE, Alves JL, Neto R. Influence of Infiltration Post-Processing in Binder Jetting Technology in Advanced Structured Materials, Lucas F.M. da Silva, Editor. Springer: Porto, Portugal, 2016, 416.
49. Kuntze RA. Gypsum: Connecting Science and Technology. ASTM International, 2009.